



OPEN

Detecting type 2 diabetes mellitus cognitive impairment using whole-brain functional connectivity

Jinjian Wu^{1,2}, Yuqi Fang², Xin Tan^{1,3}, Shangyu Kang¹, Xiaomei Yue¹, Yawen Rao¹, Haoming Huang³, Mingxia Liu², Shijun Qiu³✉ & Pew-Thian Yap²✉

Type 2 diabetes mellitus (T2DM) is closely linked to cognitive decline and alterations in brain structure and function. Resting-state functional magnetic resonance imaging (rs-fMRI) is used to diagnose neurodegenerative diseases, such as cognitive impairment (CI), Alzheimer's disease (AD), and vascular dementia (VaD). However, whether the functional connectivity (FC) of patients with T2DM and mild cognitive impairment (T2DM-MCI) is conducive to early diagnosis remains unclear. To answer this question, we analyzed the rs-fMRI data of 37 patients with T2DM and mild cognitive impairment (T2DM-MCI), 93 patients with T2DM but no cognitive impairment (T2DM-NCI), and 69 normal controls (NC). We achieved an accuracy of 87.91% in T2DM-MCI versus T2DM-NCI classification and 80% in T2DM-NCI versus NC classification using the XGBoost model. The thalamus, angular, caudate nucleus, and paracentral lobule contributed most to the classification outcome. Our findings provide valuable knowledge to classify and predict T2DM-related CI, can help with early clinical diagnosis of T2DM-MCI, and provide a basis for future studies.

Type 2 diabetes mellitus (T2DM), accounting for the highest percentage of adults with diabetes, is a series of chronic endocrine and metabolic abnormalities. T2DM is related to clinical complications such as cognitive impairment (CI) and dementia. T2DM patients are at a 1.5 times higher risk for dementia or cognitive decline than individuals without diabetes^{1,2}. Patients with diabetes manifest brain atrophy and microvascular disease in magnetic resonance imaging (MRI) exams³. However, factors contributing to the onset and progression of brain complications in patients with T2DM remain unclear. Therefore, there is an urgent need to identify these factors and early detection as the prevalence of T2DM is rising with population aging.

Increasing evidence indicates that patients with T2DM present structural and functional brain pathological changes⁴. In China, the prevalence of mild cognitive impairment (MCI), the prodromal stage of Alzheimer's disease (AD), is 45% (ranges from 21.8 to 67.5%) in older patients with T2DM, substantially higher than 14.71% in older populations without T2DM. Prevalence is higher in older women⁵⁻⁷. MCI can gradually develop into moderate or severe CI and even AD⁵. Since AD cannot be completely cured, early detection and pharmacological and behavioral interventions of MCI are crucial for reducing the risk for AD⁸.

In the past 20 years, high-precision brain imaging techniques, such as structural, functional, and diffusion MRI as well as positron emission tomography (PET), have been demonstrated to be effective for investigating brain changes in patients with T2DM and MCI (T2DM-MCI)⁹. For instance, the blood oxygen level-dependent (BOLD) signal in fMRI, which reveals hemodynamic changes associated with neural activities, has been used to detect altered functional connectivity (FC) in patients with T2DM-MCI^{5,10-12}. Diffusion tensor imaging (DTI), which quantifies the diffusion anisotropy of water molecules in white matter (WM), has been used to explore disruptions of structural network connectivity¹³⁻¹⁶. PET has been used to capture metabolic changes in the brain for early diagnosis¹⁷.

FC can be employed to reflect the functional condition of the brain, diagnose neurodegenerative diseases, and provide in-depth insights into pathophysiological mechanisms^{8,18-20}. Region-specific FC provides useful features for T2DM-MCI classification. However, existing T2DM-MCI classification methods based on FC have limited accuracy of less than 70.0%^{21,22}. Therefore, further effort is needed to improve the specificity and accuracy. The eXtreme Gradient Boosting (XGBoost)^{23,24}, which improves classification based on iterative learning of weak classifiers. On a single machine, XGBoost is more than tenfold faster than existing popular solutions,

¹The First School of Clinical Medicine, Guangzhou University of Chinese Medicine, Guangzhou, Guangdong, China. ²Department of Radiology and Biomedical Research Imaging Center, University of North Carolina, Chapel Hill, NC, USA. ³Department of Radiology, The First Affiliated Hospital of Guangzhou University of Chinese Medicine, Guangzhou, Guangdong, China. ✉email: qiu-sj@163.com; ptyap@med.unc.edu

with scalability to handle billions of samples. Model learning can be accelerated with parallel and distributed computing²³. XGBoost is used in various applications^{25,26} owing to its high efficiency and accuracy. However, no previous study has used XGBoost for classifying patients with T2DM-MCI based on FC features. Therefore, the aim of the present study was to identify meaningful features to specifically distinguish T2DM-MCI.

Based on previous evidence, this study focused on the following objectives: (1) implement an efficient XGBoost classifier for T2DM-MCI classification; and (2) determine brain regions that distinguish patients with T2DM-MCI, providing a basis for early clinical diagnosis and interventional treatments.

Results

Clinical and neuropsychological results. A total of 199 participants underwent MRI, clinical blood, and neuropsychological scale tests and fulfilled the inclusion criteria. The mean ages at scanning for the T2DM-MCI, T2DM-NCI, and NC groups were 46.17 ± 8.67 , 50.78 ± 8.28 , and 46.30 ± 10.40 years, respectively. The demographic, clinical, and neuropsychological characteristics of the 199 participants are summarized in Tables 1,2,3. There were no significant differences between the T2DM-MCI, T2DM-NCI, and NC groups in sex, age, or educational level ($p > 0.05$). There were no statistically significant differences between the T2DM-MCI and T2DM-NCI groups in glycosylated hemoglobin levels, body mass index (BMI), or fasting blood glucose levels ($p > 0.05$). BMI was significantly different between the T2DM-NCI and NC groups ($p = 0.001$). Compared with the T2DM-MCI group, the T2DM-NCI and NC groups had higher levels of auditory verbal learning test (AVLT, immediate: $p = 0.002$ and $p = 0.003$; 5 min: $p = 0.000$ and $p = 0.000$; delay: $p = 0.000$ and $p = 0.000$; recall: $p = 0.000$ and $p = 0.000$), digit span test (reverse, $p = 0.000$ and $p = 0.001$), Montreal Cognitive Assessment-B (MoCA-B, $p = 0.000$ and $p = 0.000$), digit symbol substitution (DSST, $p = 0.000$ and $p = 0.000$), and lower levels of grooved pegboard test (GPT, L: $p = 0.005$ and $p = 0.007$; R: $p = 0.000$ and $p = 0.000$). There were no statistically significant differences in the other neuropsychological test outcomes among the three groups ($p > 0.05$) (Tables 1,2,3).

Classification performance. A summary of classification performance using XGBoost is shown in Table 4 in terms of accuracy (ACC), the area under the curve (AUC), sensitivity (SEN), specificity (SPE), precision (PRE),

	T2DM-NCI		T2DM-MCI		NC		<i>p</i>
	Mean	SD	Mean	SD	Mean	SD	
Age (years)	46.17	8.67	50.78	8.28	46.3	10.403	0.058
Gender (M/F)	60/33		23/14		43/26		0.969*
Educational level (years)	12.10	3.45	11.27	3.90	12.05	3.47	0.762
BMI (kg/m ²)	24.70	2.93	23.43	3.12	23.05	2.76	0.003*

Table 1. Demographic results of T2DM-MCI, T2DM-NCI and NC groups. Data are shown as mean \pm standard deviation (SD) and were analyzed using independent sample t-tests. BMI body mass index. *Pearson's Chi-square test (2-sided). *Statistically significant different ($p < 0.05$).

	T2DM-NCI		T2DM-MCI		NC		<i>p</i>
	Mean	SD	Mean	SD	Mean	SD	
AVLT (immediate)	23.71	4.92	20.41	5.51	23.84	5.15	0.008*
AVLT (immediate)	23.71	4.92	20.41	5.51	23.84	5.15	0.008*
AVLT (5 min)	9.46	2.27	7.50	2.67	10.09	4.11	0.000*
AVLT (delay)	9.14	2.46	6.97	2.96	9.28	2.23	0.000*
AVLT (recall)	11.07	2.10	8.21	3.97	11.03	1.88	0.000*
TMT-A	47.05	23.25	59.68	19.59	51.25	21.75	0.000*
TMT-B	40.18	17.01	48.76	15.87	43.23	16.72	0.009*
DST (direct)	7.85	1.47	7.32	1.61	10.08	9.16	0.102
DST (reverse)	4.95	1.26	3.89	1.59	5.10	1.64	0.000*
MoCA-B	27.51	1.55	24.05	0.85	27.52	1.54	0.000*
MMSE	28.49	1.54	27.83	1.84	28.32	1.69	0.170
DSST	49.75	12.89	35.03	12.77	48.24	14.83	0.000*
GPT (R)	74.17	13.53	90.70	27.53	68.49	14.17	0.000*
GPT (L)	81.60	15.25	93.81	30.89	80.10	18.22	0.023*

Table 2. Neuropsychological results of T2DM-MCI, T2DM-NCI and NC groups. Data are shown as mean \pm standard deviation (SD) and were analyzed using independent sample t-tests. AVLT California-Los Angeles auditory verbal learning test, TMT trail-making test, DST digit span test, MoCA montreal cognitive assessment, MMSE mini-mental state examination, DSST digit symbol substitution, GPT grooved pegboard test, L left, R right. *Data was considered significantly different ($p < 0.05$).

	T2DM-NCI		T2DM-MCI		NC		<i>p</i>
	Mean	SD	Mean	SD	Mean	SD	
HbA1c (%)	9.25	2.56	8.75	2.15	NA	NA	0.522
DBP (mmHg)	126.42	16.62	127.79	19.96	123.48	19.04	0.273
SBP (mmHg)	82.74	14.00	82.25	10.72	82.40	11.12	0.783
FBG (mmol/L)	8.93	2.96	7.95	2.68	4.50	0.76	0.000*
FSI (uIU/mL)	11.25	9.79	14.08	16.05	NA	NA	0.507
TG (mmol/L)	2.67	2.58	3.25	3.83	NA	NA	0.775
TC (mmol/L)	4.76	1.03	4.99	1.06	NA	NA	0.694
LDL (mmol/L)	3.02	0.99	3.15	0.88	NA	NA	0.785
ACR (mg/g)	30.00	96.60	22.18	51.45	NA	NA	0.068
mALB (mg/L)	29.15	80.94	24.79	50.62	NA	NA	0.221
24 h UPRO (G/24 h)	0.19	0.23	0.17	0.14	NA	NA	0.436
M-TP (mg/L)	101.71	68.93	102.18	79.54	NA	NA	0.995
C-Peptide (ng/mL)	2.27	1.22	2.31	1.26	NA	NA	0.674

Table 3. Clinical results of T2DM-MCI, T2DM-NCI and NC groups. Data are shown as mean \pm standard deviation, independent sample t-tests. *Data was considered significant different ($p < 0.05$). *HbA1c* hemoglobinA1c, *DBP* diastolic blood pressure, *SBP* systolic blood pressure, *FBG* fasting blood glucose, *FSI* fasting serum insulin, *TG* triglyceride, *TC* total cholesterol, *LDL* low-density lipoprotein, *ACR* albumin/creatinine ratio, *mALB* microalbuminuria, *24 h UPRO* 24-h urinary protein, *M-TP* micro total protein.

	ACC (%)	AUC (%)	F1 (%)	SEN (%)	SPE (%)	PRE (%)
T2DM-NC vs. T2DM-MCI	87.91 \pm 1.04	81.99 \pm 8.30	73.95 \pm 2.54	61.67 \pm 4.56	98.06 \pm 1.77	93.06 \pm 6.36
T2DM-NC vs. NC	80.00 \pm 0.83	84.14 \pm 3.44	76.24 \pm 1.48	75.65 \pm 7.28	83.23 \pm 6.20	77.58 \pm 4.86
T2DM-NC vs. T2DM-MCI and NC	69.39 \pm 1.27	80.07 \pm 0.76	68.11 \pm 0.87	69.39 \pm 1.27	78.14 \pm 1.33	70.90 \pm 1.54

Table 4. Classification performance in T2DM-MCI, T2DM-NC and NC differentiation. *ACC* accuracy, *AUC* the area under the receiver operating characteristic curve, *SEN* sensitivity, *SPE* specificity, *PRE* precision.

and F1²⁷. We constructed the XGBoost model to classify all three groups and pairwise classifications between two groups. The XGBoost model did not perform well in the three classification categories (ACC = 69.39%, AUC = 80.07%, SEN = 69.39%, SPE = 78.14%, PRE = 70.90%, and F1 = 68.11%); however, the model achieved peak performance in discriminating between the two classification categories (T2DM-NCI versus T2DM-MCI: ACC = 87.91%, AUC = 81.99%, SEN = 61.67%, SPE = 98.06%, PRE = 93.06%, and F1 = 73.95%; T2DM-NCI versus NC: ACC = 80.00%, AUC = 84.14%, SEN = 75.65%, SPE = 83.23%, PRE = 77.58%, and F1 = 76.24%).

Connections contributive to classification. Out of 4,005 connections, 511 connections provided useful features for classification (analysis of variance (ANOVA) with Bonferroni correction, $p < 0.05$). After using the XGBoost model for classification, we traced the data to further explore and analyze the 511 functional connections. Many functional connections were connected through the same brain region; precisely, we observed the aggregation of connection features. We found that the following eight areas are most discriminative: left caudate nucleus (CAU.L, 14.68%), right caudate nucleus (CAU.R, 12.13%), left angular gyrus (ANG.L, 10.76%), left thalamus (THA.L, 7.83%), right paracentral lobule (PCL.R, 7.63%), right thalamus (THA.R, 7.44%), right angular gyrus (ANG.R, 6.65%), and left paracentral lobule (PCL.L, 4.7%). There were more than 70% of connections to CAU (26.81%), ANG (17.42%), THA (15.26%), and PCL (12.33%). The FC of these regions contribute most to T2DM-MCI classification (71.82% total, see Table 5 and Fig. 1).

Association between classification features and clinical variables. To better understand the relationship between the characteristics of the clinical development of T2DM-MCI, we further analyzed the correlation between imaging data and clinical variables (Bonferroni correction). The correlations between significant cognitive function scores and different brain regions were analyzed using Pearson's correlation for three groups (Fig. 2). ANG.L was positively correlated with TMT-B ($r = 0.224$, $p = 0.043$), ANG.R is negatively correlated with BMI ($r = -0.215$, $p = 0.042$). PCL.R was positively correlated with AVLT (5 min) ($r = 0.267$, $p = 0.015$) and AVLT (delay) ($r = 0.233$, $p = 0.037$). THA.L was positively correlated with educational level ($r = 0.236$, $p = 0.027$). MoCA was positively correlated with DSST ($r = 0.392$, $p = 0.000$) and educational level ($r = 0.204$, $p = 0.007$). There was no significant correlation between other variables and the brain regions.

Brain region	Total ratio (%)	Subregion	Ratio (%)
CAU	26.81	CAU.L	14.68
		CAU.R	12.13
ANG	17.42	ANG.L	10.76
		ANG.R	6.65
THA	15.26	THA.L	7.83
		THA.R	7.44
PCL	12.33	PCL.L	4.70
		PCL.R	7.63

Table 5. Brain regions most contributive to classification. *CAU* caudate nucleus, *ANG* angular gyrus, *THA* thalamus gyrus, *PCL* paracentral lobule, *L* left, *R* right.

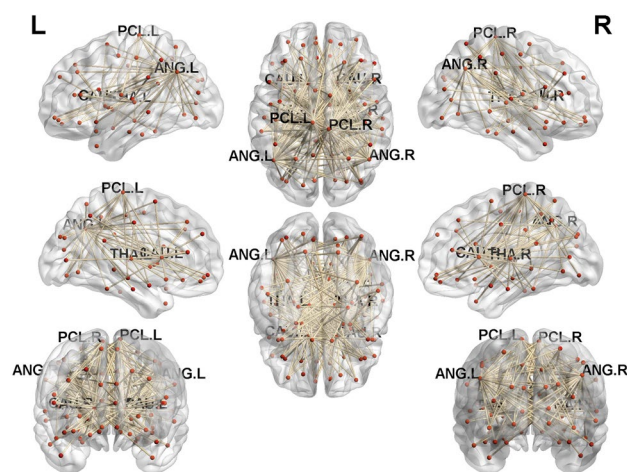


Figure 1. Significant connections rendered on the surface of the automated anatomical labeling atlas in BrainNet viewer. *THA* thalamus, *ANG* angular gyrus, *CAU* caudate nucleus, *PCL* paracentral lobule, *L* left, *R* right.

Discussion

T2DM-MCI has a relatively low clinical diagnostic rate owing to its subtle onset and lack of clinical diagnostic approach. This study examined whether FC has discriminative features for accurately detecting T2DM-MCI using XGBoost patterns. The XGBoost algorithm is an accurate and efficient classification algorithm used in data mining with good performance. XGBoost has been applied for early diagnoses of diseases such as tuberculosis, epilepsy, kidney disease, and breast cancer^{28–32}. Notably, this study is the first to apply whole-brain FC for detecting T2DM-MCI using the XGBoost model. Our model yields better classification performance (87.91% accuracy) than that of previous studies^{21,22}. Using only 23 patients with T2DM and CI, Chen et al.²¹ used high-order FC for differentiating healthy controls from patients with T2DM and CI (79.17% accuracy) and patients with T2DM without CI (59.62% accuracy). With only 16 T2DM-MCI, Shi et al. employed large-scale FC to predict MoCA scores with a connectome-based predictive model and support vector machine, achieving AUC values (T2DM-NCI vs. T2DM-MCI) of 0.65–0.70, which was significantly lower than that obtained by our method (0.82 in AUC). Moreover, our sample size was larger than those of previous studies^{21,22,33}, including 199 participants in total.

T2DM is typically related to an increased risk of CI and dementia. Patients with T2DM may experience memory, language, attention, concentration, reaction, and executive function decline^{1,34}. Nevertheless, researchers are still unsure of the exact pathophysiology underlying T2DM-related cognitive dysfunction, delaying the development of preventive treatments. We further found that the FC of *THA*, *ANG*, *CAU*, and *PCL* was highly discriminative in distinguishing T2DM-MCI, T2DM-NCI, and NC.

THA is a relay station or hub transmitting information between subcortical, cortical, and cerebellar areas³⁵. *THA* declines with normal aging³⁶. There may be no obvious structural damage, however, it develops thalamocortical FC impairment in patients with T2DM²¹. In our preliminary study³⁷, patients with T2DM without CI already had abnormalities in the dynamic FC of *THA*, as revealed by a significant decrease in connectivity between the right executive control network and *THA.L*. Abnormal thalamic connectivity is associated with CI. Thalamic connectivity is likely to be impaired in patients with T2DM and CI, which is consistent with our results^{21,38,39}. When undergoing external working memory tasks, the corresponding working memory brain regions are activated, and the right hippocampal/parahippocampal gyrus and *THA* are abnormally activated predominantly

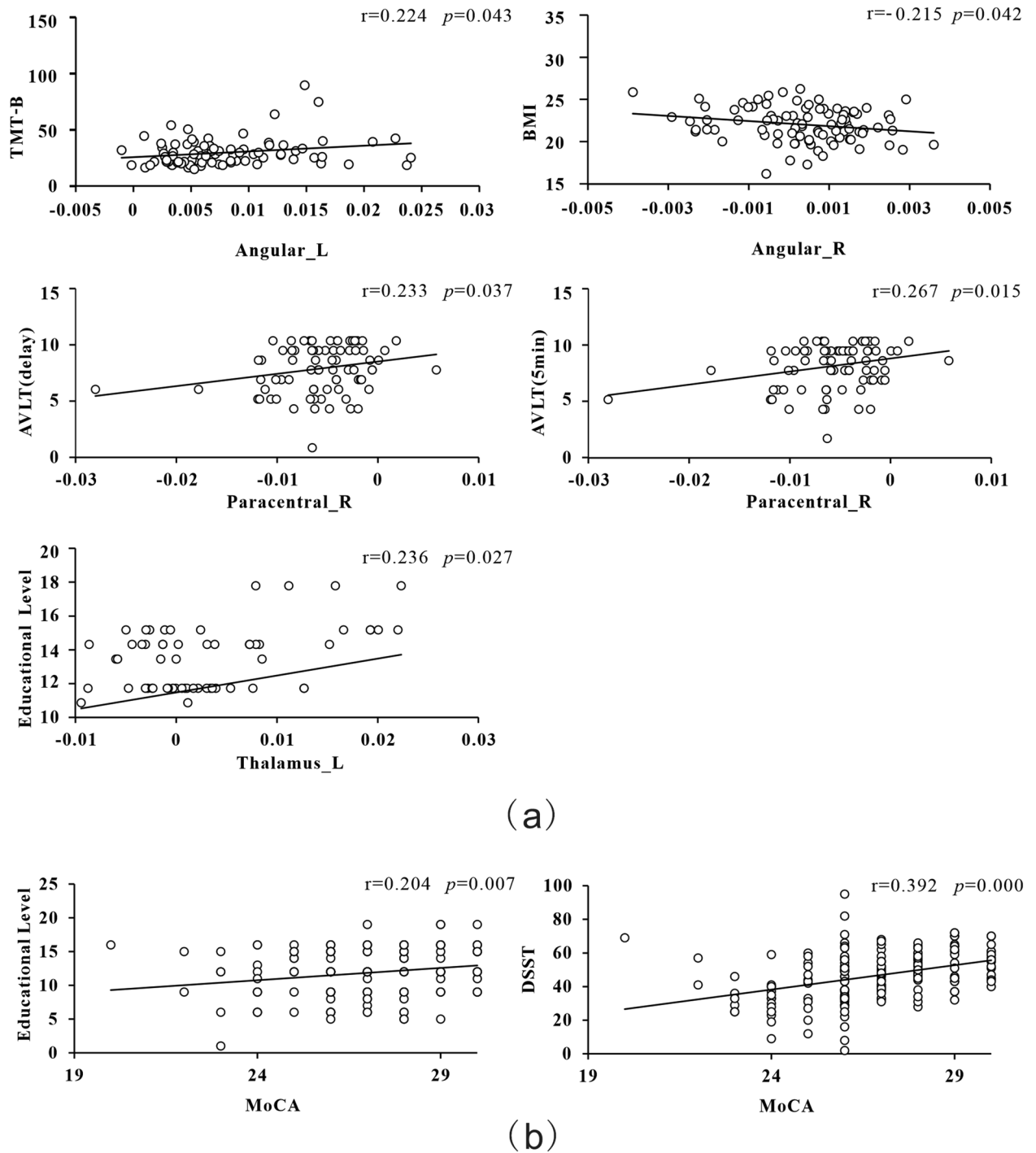


Figure 2. Associations between neuropsychological test scores and functional connectivity. Partial correlation was used to determine the relationship between neuropsychological test scores and functional connectivity. (a) Correlation of functional connectivity with neuropsychological test scores (b) Correlation between neuropsychological test scores. *TMT* trail-making test, *BMI* body mass index, *AVLT* World Health Organization University of California-Los Angeles auditory verbal learning test, *MoCA-B* montreal cognitive assessment-B, *DSST* digit symbol substitution test, *L* left, *R* right.

in the right cerebral hemisphere⁴⁰. This indicates that *THA* is involved in processing working memory, and *FC* is already impaired before the onset of *CI* in patients with *T2DM*. *ANG* is associated with complex language functions and linked to other cognitive domains such as representational and semantic memory⁴¹. Patients with *T2DM* exhibit significantly thinner *ANG* cortical thickness⁴², reduced cerebral blood flow⁴³, and less spontaneous neuronal activities⁴⁴. Moreover, abnormal *FC* in *THA* and *ANG* because of diabetes causes various cognitive dysfunctions, including *AD/VaD*^{38,45,46}. Compared with *NC*, bilateral *ANG* in patients with *T2DM* exhibit

abnormal FC with multiple brain regions, and the FC of ANG with multiple brain regions positively correlated with MoCA, suggesting that the broad functional disconnectedness of ANG may play an essential role in the neuropathology of patients with T2DM-MCI⁴⁵.

CAU is associated with memory and learning abilities⁴⁷ as well as executive and cognitive processes⁴⁸. CAU and the cerebellum function as a network that controls behavior⁴⁹. FC between the CAU and hippocampus, which is an important anatomic basis for learning and memory, is implicated in altered white matter structure in patients with T2DM⁵⁰. CAU has extensive connections to cortical and subcortical structures that serve complex regulation of motor function, cognition, and emotion⁵¹. In patients with T2DM, the grey matter volume of CAU is significantly reduced⁴², and the microstructure is abnormal⁵⁰. The characteristics of the abnormalities are significantly associated with the duration of T2DM. In addition, the activation of the left CAU, hippocampus, and parahippocampal gyrus is weaker in T2DM-MCI than in normal controls under memory task stimulation⁴⁰. Consistent with the previous studies mentioned above, the abnormality of FC of the CAU in our findings indicates impaired cognitive functions in patients with T2DM. In addition, PCL is associated with motor and sensory innervation of the contralateral lower extremities as well as the regulation of physiological functions. However, FC in PCL is affected in cognition-related diseases, such as vascular cognitive impairment. Sun et al. found that the most obvious regions showing connectivity deficits were between several regions, including PCL, and CAU. R⁵². They also showed impaired connectivity in the default mode network, and PCL with CAU.R. PCL was also discriminative as a region of interest (ROI) feature in the T2DM classification³³. Furthermore, during the analysis of the internal connectivity of the left executive control network, ANG.L and PCL.L had significantly decreased connectivity with other brain regions in the network. In the external network connectivity analysis, significant differences were found between the left executive control network and ANG.R/PCL.L. In addition, significant differences were observed between the right executive control network and PCL.R/ANG.R. Furthermore, significant differences were found between the precuneus network and CAU.R/ANG³⁷. In summary, THA, ANG, CAU, and PCL are highly sensitive to T2DM. They play essential roles in the early diagnosis of T2DM-MCI.

Educational level, age, BMI, blood pressure, and blood glucose levels are key factors influencing MCI in patients with T2DM. Correlation analysis showed that THA.L and MoCA were positively correlated with educational level, suggesting that highly-educated people have a lower risk of developing MCI^{53,54}. Lower FC strength in ANG. R was associated with higher BMI. We also found that higher cognition scores were positively correlated with higher FC in PCL.R and ANG.L. This corresponds with previous findings^{21,55} that people with higher FC in PCL.R and ANG.L have a smaller risk of developing MCI.

Our study has some advantages. First, this study is the first to apply the XGBoost model to classify T2DM-MCI and achieve a good classification performance. Second, our analysis was based on whole-brain FC, unlike previous studies that were based on brain regions or predefined networks^{8,21,56,57}. Third, we found that THA, ANG, CAU, and PCL demonstrated significant discriminative power in T2DM-MCI detection. However, our study has some limitations. First, the overall T2DM study sample was below 200; the number of T2DM-MCI was small. Therefore, multicenter data collection should be considered to expand the sample size in future studies. Second, this classification study extracted different characteristic connections based on all participants and applied the features to training classification, which has the problem of cross-validation and is slightly limited in the subsequent application. Subsequent studies can consider separating the training and test sets and conducting feature extraction so that the data results can be more objective and random. Third, our research is only a cross-sectional study. We believe that combining follow-up and longitudinal studies will better explain the mechanism of accelerated neurodegenerative changes in T2DM-MCI.

Conclusion

This study proposes a novel framework to pool the connectivity features extracted from whole brain FC for detecting T2DM-MCI. The current study is the first attempt to use the XGBoost model to detect T2DM-MCI, which significantly enhances the prediction accuracy of the model. We show that the FC within THA, ANG, CAU, and PCL provides major information for detecting T2DM-MCI. Our results affirm that FC contains clinically relevant cognition-related information. Therefore, it is a potential biomarker for assessing the degree of cognitive decline. Overall, our findings provide valuable knowledge for classifying and predicting T2DM-related CI. These results have clinical implications in patients with T2DM. It can help in early clinical diagnosis and provides a basis for future studies.

Methods

Two hundred and ten individuals were willing to join this study (May 10, 2021, to July 1, 2022). The exclusion criteria for the two groups were as follows: type 1 diabetes mellitus, impaired fasting glucose or impaired glucose tolerance⁵⁸, hypertension, hypoglycemia (blood sugar levels < 3.9 mmol/L), hyperlipidemia, serious eye diseases (e.g., blindness), symptoms of neurological conditions (e.g., cerebral infarction or hemorrhage), history of neurological abnormality (e.g., Parkinson's disease), severe head injuries or chronic head discomfort (e.g., migraine), BMI > 31 kg/m², left- or mixed-handedness, substance (tobacco, alcohol, or psychoactive drug) abuse, taking medications that may affect cognition and memory within 6 months, specific abnormalities detected on conventional MRI scans or any other factors that may influence brain structure or function (e.g., extreme physical weakness, chronic infections, and other endocrine diseases). Patients with T2DM were diagnosed by two experienced endocrinologists following international clinical standards⁵⁹. MCI was evaluated via Mini-Mental State Examination (MMSE) and MoCA-B (21 ≤ MoCA-B score < 26, and MMSE score > 24 were diagnosed with MCI)^{60,61}.

Participants with brain tumors (n = 3), neuropsychiatric diseases (n = 4) (e.g., major depression or schizophrenia), or developmental disorders (n = 4) were excluded. Finally, 37 patients with T2DM-MCI, 93 patients with

T2DM-NCI, and 69 NC were enrolled in this study. The source of patients with T2DM and NC corresponded with our previous study³⁷. This study was approved by the ethics committee of The First Affiliated Hospital of Guangzhou University of Chinese Medicine (ID: NO. JY [2020] 288). Written informed consent was obtained from all participants. In addition, the study was conducted following approved guidelines.

Demographic, clinical, and neuropsychological assessments. Demographic assessments include age, sex, educational level, past medical history, height, weight and medication history. Clinical assessments include HemoglobinA1c (HbA1c), C-Peptide, systolic blood pressure (SBP), diastolic blood pressure (DBP), total cholesterol (TC), triglyceride (TG), fasting serum insulin (FSI), low-density lipoprotein (LDL), fasting blood glucose (FBG), microalbuminuria (mALB), albumin/creatinine ratio (ACR), micro total protein (M-TP), 24-h urinary protein (24 h UPRO). Neuropsychological assessments include MoCA-B, MMSE, digit span test (DST), AVLT, TMT, GPT, and DSST which can be used to assess cognitive ability.

MRI data acquisition. A Siemens (Munich, Germany) 3 T Prisma scanner with a standard 64-channel head coil was used to acquire fMRI imaging. All participants were placed in the supine position and tried their best to keep heads as still as possible while acquiring images. The detailed parameters of the multi-slice T2-weighted echo-planar imaging (EPI) sequence were as follows: TR = 2000 ms; TE = 30 ms; FOV = 100 mm; flip angle = 90°; matrix dimensions = 64 × 64; slice thickness = 3.5 mm; and number of slices = 33. Three-dimensional T1-weighted images were acquired with the following parameters: TR = 2,530 ms; TE = 2.98 ms; FOV = 256 × 224 mm²; inversion time = 1,100 ms; flip angle = 7°; matrix size = 224 × 256; sagittal slices = 192; slice thickness = 1.0 mm; and voxel size = 0.5 × 0.5 × 1 mm³. The BOLD-fMRI gradient EPI sequence acquisition parameters were as follows: TR = 500 ms; TE = 30 ms; matrix dimensions = 64 × 64; FOV = 244 mm × 244 mm; slices thickness = 3.5 mm; voxel size = 3.5 mm × 3.5 mm; number of slices = 960, and scan time = 8 min.

MRI image pre-processing. For fMRI data, the pre-processing was performed using SPM12 (Wellcome Department of Imaging Neurosciences, University College London, UK, <http://www.fil.ion.ucl.ac.uk/spm>), and the statistical analyses of imaging data were performed using GRETNA (GRETNA v2.0) in Matlab R2021b. First, the first 10-time point-scanned images were removed owing to the instability of the magnetic field at the beginning of the scan. Second, all functional images were realigned to the first image to correct head movement. All participants met the criteria of < 2 mm translation and < 2° rotation in any direction. Otherwise, their data were excluded. Third, the functional images were normalized to the MNI space using DARTEL and resampled to a 3 × 3 × 3 mm³ voxel size⁶². Fourth, we used an anisotropic 6-mm full-width half-maximum Gaussian kernel⁶³ for spatial smoothing of the obtained images. Fifth, we detrended and removed linear trends. Sixth, we removed covariates, excluding white matter, grey matter, and cerebrospinal fluid influences. Seventh, 0.01–0.08 Hz bandpass filtering was used to remove high and low-frequency signals. Eighth, we removed the FD_Threshold > 0.5 mm time points by “scrubbing” 1-time point before and 2-time points after. In summary, the pre-processing procedures included slice timing correction, realignment, normalization, smoothing, detrending, filtering, and scrubbing.

Statistical analyses. All statistical analyses were performed using the SPSS software package (version 26.0). The measurement data of each group were described by mean ± standard deviation. The demographic, clinical, and neuropsychological assessment scores of the three groups were compared using multiple independent sample ANOVA⁶⁴. Categorical data were evaluated using Chi-square analysis. Paired-sample t-tests were used for pre- and post-treatment intragroup comparisons. In addition, a partial test was used to examine the relationship between imaging indices, cognitive tests, and clinical data. $p < 0.05$ was used as the statistical significance level.

Classification based on the ANOVA-XGBoost model. *Feature abstraction based on FC network.* The pre-processed fMRI BOLD data has dimensions of 950 × 90, where 950 denotes the number of time points in each fMRI scan, and 90 means the number of ROI derived from the Automated Anatomical Labelling atlas. We calculated the mean BOLD signals for each brain ROI by averaging the time series over all voxels within the ROI. Subsequently, based on the pre-processed fMRI data, we used the Pearson correlation coefficient⁶⁵ to build an FC network for each participant in a matrix size of 90 × 90. Every node represented a brain ROI, and every edge measured the linear correlation between any pair of ROI.

Subsequently, we flattened the upper triangle elements of FC, thereby deriving a 4,005-dimensional $[(90 \times 90 - 90) / 2]$ vector for each participant. However, these features may be redundant for classifying participants into the three experimental groups. Therefore, we applied ANOVA and Bonferroni correction analysis to extract features showing significant differences ($p < 0.05$) among the three groups. Finally, we generated 511 discriminative features for further classification.

Illustration of XGBoost model. The XGBoost model²³ is an ensemble machine learning algorithm based on decision trees that used the gradient boosting framework with promising performance in fMRI-related classification tasks^{29,66,67}. The XGBoost model is illustrated in Fig. 3. The XGBoost model was built based on gradient boosting machines which used Gradient Boosting Trees⁶⁸ as the error predictor. In gradient boosting, we trained a predictor to predict the errors made by the original model and constructed an improved model whose output was fine-tuned based on the original prediction. The improved model is an ensemble of two predictors, i.e., the original and error predictors. We repeated this process until we achieved satisfactory prediction results.

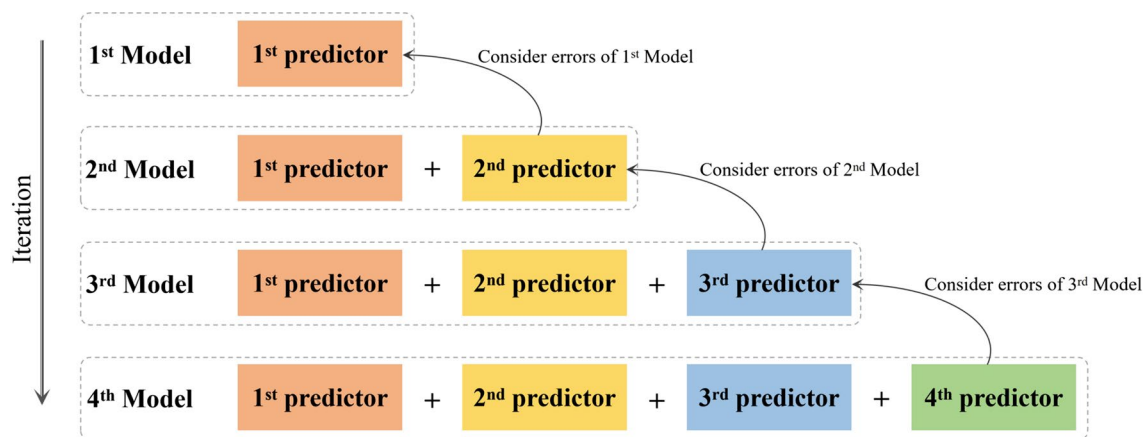


Figure 3. The illustration of XGBoost model for image classification. A predictor is trained to predict the errors made by the original model, and then construct an improved model whose output is fine-tuned based on the original prediction.

We used the XGBoost model to classify the three experimental groups, and the parameters were defined as follows: the number of gradient-boosted trees was 280; the maximum tree depth of base learners was 2; the minimum sum of sample weight required in a child was 5; the minimum loss reduction needed to make a further partition on a leaf node was 0; the subsample ratio of the training sample was 0.8; the subsample ratio for each tree's construction was 0.8; the boosting learning rate was 0.1; and the L1 regularization constraint was 0.01. The XGBoost model was implemented based on the XGBoost package in Python (Supplementary Information S1).

Experimental setting. We randomly partitioned all participants from the three groups into training and testing sets, following a 2:1 ratio, and this procedure was repeated five times. In the data division, we ensured that the three classes in both sets were equally distributed to prevent data imbalance. Five measurement metrics were adopted for model evaluation, including the AUC, ACC, F1, SEN, SPE, and PRE⁶⁹.

Data availability

The data that support the findings of this study are available from the coauthors, Jinjian Wu and Shijun Qiu, upon reasonable request.

Received: 12 October 2022; Accepted: 13 January 2023

Published online: 09 March 2023

References

- Cukierman-Yaffe, T. *et al.* Effect of dulaglutide on cognitive impairment in type 2 diabetes: An exploratory analysis of the REWIND trial. *Lancet Neurol.* **19**, 582–590 (2020).
- Srikanth, V., Sinclair, A. J., Hill-Briggs, F., Moran, C. & Biessels, G. J. Type 2 diabetes and cognitive dysfunction—towards effective management of both comorbidities. *Lancet Diabetes Endocrinol.* **8**, 535–545 (2020).
- Biessels, G. J., Nobili, F., Teunissen, C. E., Simó, R. & Scheltens, P. Understanding multifactorial brain changes in type 2 diabetes: A biomarker perspective. *Lancet Neurol.* **19**, 699–710 (2020).
- Li, W., Wang, T. & Xiao, S. Type 2 diabetes mellitus might be a risk factor for mild cognitive impairment progressing to Alzheimer's disease. *Neuropsychiatr. Dis. Treat.* **12**, 2489–2495 (2016).
- Qi, D. *et al.* Default mode network connectivity and related white matter disruption in type 2 diabetes mellitus patients concurrent with amnesic mild cognitive impairment. *Curr. Alzheimer Res.* **14**, 1238–1246 (2017).
- Xue, J., Li, J., Liang, J. & Chen, S. The prevalence of mild cognitive impairment in China: A systematic review. *Aging Dis.* **9**, 706–715 (2018).
- You, Y. *et al.* The prevalence of mild cognitive impairment in type 2 diabetes mellitus patients: A systematic review and meta-analysis. *Acta Diabetol.* **58**, 671–685 (2021).
- Chen, X. *et al.* Extraction of dynamic functional connectivity from brain grey matter and white matter for MCI classification. *Hum. Brain Mapp.* **38**, 5019–5034 (2017).
- Lu, M., Guo, Z., Gao, Z., Cao, Y. & Fu, J. Multiscale brain network models and their applications in neuropsychiatric diseases. *Electronics* **11**, 3468 (2022).
- Li, C. *et al.* Type 2 diabetes mellitus may exacerbate gray matter atrophy in patients with early-onset mild cognitive impairment. *Front. Neurosci.* **14**, 856 (2020).
- Xiong, Y. *et al.* Altered regional homogeneity and functional brain networks in Type 2 diabetes with and without mild cognitive impairment. *Sci. Rep.* **10**, 1–11 (2020).
- Yu, Y. *et al.* Neurovascular decoupling in type 2 diabetes mellitus without mild cognitive impairment: Potential biomarker for early cognitive impairment. *Neuroimage* **200**, 644–658 (2019).
- Li, X. *et al.* The role of the Montreal Cognitive Assessment (MoCA) and its memory tasks for detecting mild cognitive impairment. *Neurol. Sci.* **39**, 1029–1034 (2018).
- Paschoal, A. M. Editorial for “diffusion tensor imaging reveals altered topological efficiency of structural networks in type-2 diabetes patients with and without mild cognitive impairment”. *J. Magn. Reson. Imaging* **55**, 928–929 (2022).
- Sun, Q. *et al.* Alterations of white matter integrity and hippocampal functional connectivity in type 2 diabetes without mild cognitive impairment. *Front. Neuroanat.* **12**, 21 (2018).

16. Xiong, Y. *et al.* Application of neurite orientation dispersion and density imaging to characterize brain microstructural abnormalities in type-2 diabetics with mild cognitive impairment. *J. Magn. Reson. Imaging* **50**, 889–898 (2019).
17. Ciudin, A. *et al.* Retinal microperimetry: A new tool for identifying patients with type 2 diabetes at risk for developing Alzheimer disease. *Diabetes* **66**, 3098–3104 (2017).
18. Chen, X. *et al.* High-order resting-state functional connectivity network for MCI classification. *Hum. Brain Mapp.* **37**, 3282–3296 (2016).
19. Liang, P. *et al.* Disruption of cortical integration during midazolam-induced light sedation. *Hum. Brain Mapp.* **36**, 4247–4261 (2015).
20. Qiao, L. *et al.* Estimating functional brain networks by incorporating a modularity prior. *Neuroimage* **141**, 399–407 (2016).
21. Chen, Y. *et al.* Classification of type 2 diabetes mellitus with or without cognitive impairment from healthy controls using high-order functional connectivity. *Hum. Brain Mapp.* **42**, 4671–4684 (2021).
22. Shi, A.-P. *et al.* Large-scale functional connectivity predicts cognitive impairment related to type 2 diabetes mellitus. *World J. Diabetes* **13**, 110–125 (2022).
23. Chen, T. & Guestrin, C. XGBoost: A scalable tree boosting system. in *Proceedings of the ACM SIGKDD International Conference on Knowledge Discovery and Data Mining* vols 13–17-Aug 785–794 (ACM, 2016).
24. Mackey, L., Bryan, J. & Mo, M. Y. Weighted Classification Cascades for Optimizing Discovery Significance in the HiggsML Challenge. in *NIPS 2014 Workshop on High-energy Physics and Machine Learning* 129–134 (PMLR, 2014).
25. Devan, P. & Khare, N. An efficient XGBoost–DNN-based classification model for network intrusion detection system. *Neural Comput. Appl.* **32**, 12499–12514 (2020).
26. Ramaneswaran, S., Srinivasan, K., Vincent, P. M. D. R. & Chang, C. Y. Hybrid inception v3 XGBoost model for acute lymphoblastic leukemia classification. *Comput. Math. Methods Med.* **2021**, 1–10 (2021).
27. Sokolova, M., Japkowicz, N. & Szpakowicz, S. Beyond accuracy, F-score and ROC: A family of discriminant measures for performance evaluation. in *AAAI Workshop - Technical Report* vol. WS-06–06 24–29 (Springer, 2006).
28. Ren, X., Guo, H., Li, S., Wang, S. & Li, J. A novel image classification method with CNN-XGBoost model. in *Lecture Notes in Computer Science (including subseries Lecture Notes in Artificial Intelligence and Lecture Notes in Bioinformatics)* vol. 10431 LNCS 378–390 (Springer, 2017).
29. Torlay, L., Perrone-Bertolotti, M., Thomas, E. & Baciu, M. Machine learning–XGBoost analysis of language networks to classify patients with epilepsy. *Brain Inf.* **4**, 159–169 (2017).
30. Ogunleye, A. & Wang, Q. G. XGBoost model for chronic kidney disease diagnosis. *IEEE/ACM Trans. Comput. Biol. Bioinform.* **17**, 2131–2140 (2020).
31. Liew, X. Y., Hameed, N. & Clos, J. An investigation of XGBoost-based algorithm for breast cancer classification. *Mach. Learn. with Appl.* **6**, 100154 (2021).
32. Rahman, M., Cao, Y., Sun, X., Li, B. & Hao, Y. Deep pre-trained networks as a feature extractor with XGBoost to detect tuberculosis from chest X-ray. *Comput. Electr. Eng.* **93**, 107252 (2021).
33. Liu, Z. *et al.* Identification of cognitive dysfunction in patients with T2DM using whole brain functional connectivity. *Genom. Proteom. Bioinf.* **17**, 441–452 (2019).
34. González, H. M. *et al.* Diabetes, cognitive decline, and mild cognitive impairment among diverse Hispanics/Latinos: Study of Latinos-investigation of neurocognitive aging results (HCHS/SOL). *Diabetes Care* **43**, 1111–1117 (2020).
35. Kim, H. S. & Sasaki, J. Y. Cultural neuroscience: Biology of the mind in cultural contexts. *Annu. Rev. Psychol.* **65**, 487–514 (2014).
36. Fama, R. & Sullivan, E. V. Thalamic structures and associated cognitive functions: Relations with age and aging. *Neurosci. Biobehav. Rev.* **54**, 29–37 (2015).
37. Wu, J. *et al.* Altered functional network connectivity of precuneus and executive control networks in type 2 diabetes mellitus without cognitive impairment. *Front. Neurosci.* **16**, 887713 (2022).
38. Chen, Y.-C. *et al.* Thalamic resting-state functional connectivity: disruption in patients with type 2 diabetes. *Metab. Brain Dis.* **30**, 1227–1236 (2015).
39. Tan, X. *et al.* Micro-structural white matter abnormalities in type 2 diabetic patients: A DTI study using TBSS analysis. *Neuroradiology* **58**, 1209–1216 (2016).
40. Huang, R. R. *et al.* Spatial working memory impairment in primary onset middle-age type 2 diabetes mellitus: An ethology and BOLD-fMRI study. *J. Magn. Reson. Imaging* **43**, 75–87 (2016).
41. Humphreys, G. F., Lambon Ralph, M. A. & Simons, J. S. A unifying account of angular gyrus contributions to episodic and semantic cognition. *Trends Neurosci.* **44**, 452–463 (2021).
42. Peng, B., Chen, Z., Ma, L. & Dai, Y. Cerebral alterations of type 2 diabetes mellitus on MRI: A pilot study. *Neurosci. Lett.* **606**, 100–105 (2015).
43. Bangen, K. J. *et al.* Reduced regional cerebral blood flow relates to poorer cognition in older adults with type 2 diabetes. *Front. Aging Neurosci.* **10**, 270 (2018).
44. Wang, Z.-L. *et al.* Abnormal spontaneous brain activity in type 2 diabetic retinopathy revealed by amplitude of low-frequency fluctuations: A resting-state fMRI study. *Clin. Radiol.* **72**, 340–e1 (2017).
45. Qi, F. *et al.* Functional disconnection of the angular gyrus related to cognitive impairment in patients with type 2 diabetes mellitus. *Front. Hum. Neurosci.* **15**, 25 (2021).
46. Zhang, Y. *et al.* Sensorimotor and pain-related alterations of the gray matter and white matter in Type 2 diabetic patients with peripheral neuropathy. *Hum. Brain Mapp.* **41**, 710–725 (2020).
47. Driscoll, M. E., Bollu, P. C. & Tadi, P. Neuroanatomy, nucleus caudate. in *StatPearls [Internet]* (StatPearls Publishing, 2021).
48. Habas, C. *et al.* Distinct cerebellar contributions to intrinsic connectivity networks. *J. Neurosci.* **29**, 8586–8594 (2009).
49. Graff-Radford, J., Williams, L., Jones, D. T. & Benarroch, E. E. Caudate nucleus as a component of networks controlling behavior. *Neurology* **89**, 2192–2197 (2017).
50. Hsu, J.-L. *et al.* Microstructural white matter abnormalities in type 2 diabetes mellitus: A diffusion tensor imaging study. *Neuroimage* **59**, 1098–1105 (2012).
51. Ghaziri, J. *et al.* Subcortical structural connectivity of insular subregions. *Sci. Rep.* **8**, 8596 (2018).
52. Sun, Y. *et al.* Abnormal functional connectivity in patients with vascular cognitive impairment, no dementia: A resting-state functional magnetic resonance imaging study. *Behav. Brain Res.* **223**, 388–394 (2011).
53. Cesar, K. G., Yassuda, M. S., Porto, F. H. G., Brucki, S. M. D. & Nitrini, R. MoCA Test: normative and diagnostic accuracy data for seniors with heterogeneous educational levels in Brazil. *Arq. Neuropsiquiatr.* **77**, 775–781 (2019).
54. Freitas, S., Simões, M. R., Maróco, J., Alves, L. & Santana, I. Construct validity of the montreal cognitive assessment (MoCA). *J. Int. Neuropsychol. Soc.* **18**, 242–250 (2012).
55. Li, C. *et al.* Alterations of brain structural network connectivity in type 2 diabetes mellitus patients with mild cognitive impairment. *Front. Aging Neurosci.* **12**, 615048 (2021).
56. Lekha, S. & M., S. Real-time non-invasive detection and classification of diabetes using modified convolution neural network. *IEEE J. Biomed. Heal. Inf.* **22**, 1630–1636 (2018).
57. Ndaba, M., Pillay, A. W. & Ezugwu, A. E. An improved generalized regression neural network for type II diabetes classification. in *Lecture Notes in Computer Science (including subseries Lecture Notes in Artificial Intelligence and Lecture Notes in Bioinformatics)* vol. 10963 LNCS 659–671 (Springer, 2018).

58. Ogurtsova, K. *et al.* IDF Diabetes Atlas: Global estimates for the prevalence of diabetes for 2015 and 2040. *Diabetes Res. Clin. Pract.* **128**, 40–50 (2017).
59. Dobrescu, R. *Oxford Textbook of Endocrinology and Diabetes, 3rd Edition. Acta Endocrinologica (Bucharest)* vol. 17 (Oxford University Press, 2021).
60. Li, C. *et al.* Cortical thickness contributes to cognitive heterogeneity in patients with type 2 diabetes mellitus. *Medicine (Baltimore)*. **97**, e10858 (2018).
61. Schrag, A., Siddiqui, U. F., Anastasiou, Z., Weintraub, D. & Schott, J. M. Clinical variables and biomarkers in prediction of cognitive impairment in patients with newly diagnosed Parkinson's disease: A cohort study. *Lancet Neurol.* **16**, 66–75 (2017).
62. Berman, B. D. *et al.* Levodopa modulates small-world architecture of functional brain networks in Parkinson's disease. *Mov. Disord.* **31**, 1676–1684 (2016).
63. Thomas Yeo, B. T. *et al.* The organization of the human cerebral cortex estimated by intrinsic functional connectivity. *J. Neurophysiol.* **106**, 1125–1165 (2011).
64. Girden, E. R. *ANOVA: Repeated measures.* (Sage Publications, Inc., 1992).
65. Benesty, J., Chen, J., Huang, Y. & Cohen, I. Pearson correlation coefficient. in *Springer Topics in Signal Processing* vol. 2 1–4 (Springer, 2009).
66. Nguyen, R. D. *et al.* A comparison of machine learning classifiers for pediatric epilepsy using resting-state functional MRI latency data. *Biomed. Rep.* **15**, 1–9 (2021).
67. Xing, X. *et al.* Modeling essential connections in obsessive–compulsive disorder patients using functional MRI. *Brain Behav.* **10**, e01499 (2020).
68. Friedman, J. H. Greedy function approximation: A gradient boosting machine. *Ann. Stat.* **29**, 1189–1232 (2001).
69. Zou, K. H., O'Malley, A. J. & Mauri, L. Receiver-operating characteristic analysis for evaluating diagnostic tests and predictive models. *Circulation* **115**, 654–657 (2007).

Author contributions

Conceived and designed the work: J.W. and S. K. Analyzed data: X.T. and Y.F. Acquired the data: X. Y., Y. R., and H. H. Wrote the manuscript: J. W. and P. Y. Theoretical guidance: M.L., S. Q. All authors revised the work for important intellectual content. All authors have read and approved the manuscript.

Funding

This work is supported by grants from the National Natural Science Foundation of China—Major International (Regional) Joint Research Project (81920108019), Major Project (91649117). This work is also supported by the International Program for Postgraduates, Guangzhou University of Chinese Medicine. Pew-Thian Yap was supported in part by the United States National Institutes of Health (NIH) under grant EB006733.

Competing interests

The authors declare no competing interests.

Additional information

Supplementary Information The online version contains supplementary material available at <https://doi.org/10.1038/s41598-023-28163-5>.

Correspondence and requests for materials should be addressed to S.Q. or P.-T.Y.

Reprints and permissions information is available at www.nature.com/reprints.

Publisher's note Springer Nature remains neutral with regard to jurisdictional claims in published maps and institutional affiliations.



Open Access This article is licensed under a Creative Commons Attribution 4.0 International License, which permits use, sharing, adaptation, distribution and reproduction in any medium or format, as long as you give appropriate credit to the original author(s) and the source, provide a link to the Creative Commons licence, and indicate if changes were made. The images or other third party material in this article are included in the article's Creative Commons licence, unless indicated otherwise in a credit line to the material. If material is not included in the article's Creative Commons licence and your intended use is not permitted by statutory regulation or exceeds the permitted use, you will need to obtain permission directly from the copyright holder. To view a copy of this licence, visit <http://creativecommons.org/licenses/by/4.0/>.

© The Author(s) 2023